# Observations and modeling of San Diego beaches during El Niño

André Doria, R.T. Guza, William C O 'Reilly, Marissa L. Yates

# Observations and modeling of San Diego beaches during El Niño

André Doria[1], R.T. Guza[1], William C. O'Reilly[1], and M.L. Yates[2,3]

[1]Scripps Institution of Oceanography, La Jolla, California

[2]Saint-Venant Hydraulics Laboratory, Université Paris-Est (ENPC, EDF R&D, Cerema), Chatou, France

[3]Cerema

Corresponding author address: R.T. Guza, Scripps Institution of Oceanography, 9500 Gilman Drive, La Jolla, CA 92093. E-mail rguza@ucsd.edu

**KEY POINTS**

1) Subaerial sand levels were observed at 5 southern California beaches for 16 years.

2) Cobbles and bedrock sometimes reduced the mobility of eroded shorelines.

3) Inclusion of site-specific geological boundaries improves the performance of an equilibrium model.

**Abstract:** Subaerial sand levels were observed at five southern California beaches for 16 years, including notable El Niños in 1997-98 and 2009-10. An existing, empirical shoreline equilibrium model, driven with wave conditions estimated using a regional buoy network, simulates well the seasonal changes in subaerial beach width (e.g. the cross-shore location of the MSL contour) during non-El Niño years, similar to previous results with a 5-year time series lacking an El Nino winter. The existing model correctly identifies the 1997-98 El Niño winter conditions as more erosive than 2009-10, but overestimates shoreline erosion during both El Niños. The good skill of the existing equilibrium models in typical conditions does not necessarily extrapolate to extreme erosion on these beaches where a few meters thick sand layer often overlies more resistant layers. The modest over-prediction of the 2009-10 El Niño is reduced by gradually decreasing the model mobility of highly eroded shorelines (simulating cobbles, kelp wrack, shell hash, or other stabilizing layers). Over prediction during the more severe 1997-98 El Niño is corrected by stopping model erosion when resilient surfaces (identified with aerial imagery) are reached. The trained model provides a computationally simple (e.g. nonlinear first order differential equation) representation of the observed relationship between incident waves and shoreline change.

## 1. Introduction

Coastal communities and beaches provide abundant ecological, recreational, and socio-economic wealth [*Nicholls et al.*, 2007; *Yang et al.*, 2012; *McLachlan and Brown,* 2010]. Increasing coastal populations [*Moore et al.*, 1999], long-term climate change [*Keeling et al.,* 1995; *Rahmstorf et al.*, 2007], polar ice melt [*Dyurgerov and Meier*, 2000; *Bamber et al.*, 2009], and sea level rise (SLR) forecasts of between 0.8-2 m of SLR by 2100 have raised concerns about the long-term (e.g. centuries) fate of beaches, coastal infrastructure, and coastal cliff retreat [*Zhang et al.*, 2004, *Pfeffer et al.*, 2008; *Vermeer and Rahmstorf*, 2009; *Gallien et al.*, 2011]. At shorter time scales, accelerated coastal erosion may be caused by decadal oscillations in the frequency, severity, and tracks of storms [*Graham and Diaz,* 2001; *Allan and Komar*, 2006 & 2002; *Ruggiero et al.*, 2010a]. California, Oregon, and Washington beaches suffered severe erosion from the intense and frequent storms during the El Niños of 1997-98 and 2009-10 [*Revell et al.*, 2002, 2011; *Barnard et al.*, 2011].

Effectively managing beaches now, and in a future with potentially altered wave climates, requires quantifying the relationship between beach change and waves. However, testing of shoreline change models on the U.S. West coast has been limited. Genres of shoreline models include process-based and empirical. Process models [e.g. SBEACH, *Larson and Kraus*, 1989; XBeach, *Roelvink et al.*, 2009; and CSHORE, *Johnson et al.*, 2012] necessarily parameterize the complex physics of sediment transport with combined steady and oscillatory flows. Empirical models based on an equilibrium hypothesis tune "bulk response" parameters, and have skill in simulating observations of shoreline change on time scales of months to a few years [*Miller and Dean*, 2004; *Yates* *et al.*, 2009a; *Davidson et al.*, 2010, *Ruggiero et al.*, 2010b, *Davidson et al.*, 2013; *Splinter et al.*, 2014]. Equilibrium beach models quantify the hypotheses [*Wright et al.*, 1985] that: (a) for a constant wave field, there is an equilibrium beach morphology (the equilibrium beach) that would remain constant in time, neither eroding or accreting, (b) a beach in disequilibrium with the ambient waves changes towards the equilibrium shape, and (c) the change rate is proportional to the disequilibrium. *Miller and Dean* [2004] applied equilibrium concepts to derive

$$\frac{dS}{dt} = k(S_{eq}(t) - S(t)) \qquad (1)$$

where $S$ is the shoreline location (defined as the cross-shore position of a shallow depth contour, here Mean Sea Level (MSL)), $S_{eq}(t) - S(t)$ is the beach disequilibrium, and the empirical $k$ depends on wave energy, grain size, and other local factors. *Yates et al.* [2009a] (hereafter *Y09*) showed that an equilibrium shoreline model had skill at three southern California beaches over five years (2004-2009). *Ludka et al*. [2015] recently developed an equilibrium beach profile model using up to 10 years of observations that included the 2010 El Niño. Here, the southern California observations of previous studies [*Shepard*, 1950, *Winant et al.*, 1975; *Nordstrom and Inman*, 1975; *Flick and Waldorf*, 1984, *Yates et al.*, 2009a, 2009b, 2009c] are expanded to include additional sources spanning up to 16 years (1997-2014), including the more severe 1997-98 El Niño winter. The *Y09* shoreline model is extended by gradually decreasing the model mobility of highly eroded shorelines (coarsely accounting for cobbles and other natural armoring), and stopping erosion when a non-erodible layers (e.g. bedrock) is reached.

First, the beach sites (Section 2), and wave and sand level observations (Section 3) are described. In Section 4, observations of waves and shoreline (MSL contour) location are used to tune an equilibrium-type shoreline model. Results are discussed in Section 5, and summarized in Section 6.

## 2. Beach Sites

In southern California, wave conditions and beach sand levels vary seasonally [*Shepard*, 1950, *Winant et al.*, 1975; *Nordstrom and Inman*, 1975; *Flick and Waldorf*, 1984, *Yates et al.*, 2009a, 2009b, 2009c]. Sand elevations were measured at five San Diego County beaches (from south to north, Figure 1): Imperial Beach (4 km alongshore span), Torrey Pines (8 km), Solana Beach (2.6 km), Cardiff (2 km), and Camp Pendleton (2.5 km). Median sand sizes range between 0.15-0.28 mm (Table 1), and beach slope between 0.01-0.08 (Table 1).

Imperial Beach (Figure 1b) contains a recreational pier, two short groynes in the northern 300 m, and the Tijuana River mouth at the southern end. Most of the beach is backed by low-lying urban development and protective riprap, seawalls, and cobble berms (Figure 2). The southern 6.5 km of Torrey Pines State Beach (Figure 1c), is backed by 50-110 m high-relief sandstone cliffs, and the northern 1.5 km is fringed by riprap and the Los Peñasquitos Lagoon inlet [*Moore et al.*, 1999; *Young et al.*, 2010]. Solana Beach (Figure 1d) is backed by 25 m sandstone cliffs [*Young et al.*, 2010] often armored with seawalls and gunite. Cardiff (Figure 1d) is a straight, narrow beach that extends 2 km north from Solana Beach to the San Elijo Lagoon inlet. Riprap and public parking lots border the back beach. A 200 m long cobble berm, near the upper swash limit, is located at the southern end of the Cardiff site. The Camp Pendleton site (Figure 1b) spans 2.5 km north from the Santa Margarita River outlet, and the beach is backed by a vegetated low dune. During energetic winter waves, foreshore cobble patches (10s of meters in lateral extent) can be exposed at all beaches except Camp Pendleton, which is sandy year-round.

Digital orthographic and non-orthographic imagery was used to characterize the back beach type (e.g. seawall, hard cliff, soft dune, rip-rap, none) and the exposed beach face substrates (e.g. bedrock, cobbles, mixed, unknown) during the El Niño 2010 winter (Figure 2). The non-orthographic aerial imagery (Figure 2b) was collected near the 2010 El Niño maximum erosion (e.g. February 1-2, 2010) during low tide from a U.S. Coast Guard helicopter with a high-resolution DSLR camera. Orthographic aerial imagery was collected by Fugro EarthData, Inc. from 26 August - 29 November, 2010 using an airborne orthographic imaging system (Leica ADS40-SH52) with 2 m horizontal accuracy and 30 cm pixel resolution.

The non-orthographic 2010 winter aerial imagery was visually referenced to the orthographic imagery to estimate the horizontal locations of subaerial beach substrates exposed during El Niño 2010 erosion (colored polygons in Figure 2a). Non-erodible surfaces above the sand level included boulders, rock outcroppings and ledges, cobble berms and low relief bedrock. Features visible in 2010 above MSL (e.g. the cobbles in Figure 2b are above MSL) were assumed to continue below sand level at a steep, near-vertical slope. Low relief features exposed in 1997-98 may not have been detected in 2009-10.

The vertical elevations of exposed non-erodible surfaces were then estimated from the airborne lidar survey (February 26, 2010) occurring 24 days after the USGC aerial photo survey. Lidar and imagery based estimates of the subaerial substrate locations and types agreed qualitatively with ATV substrate surveys collected at all sites within 9 days of the aerial photo survey. Comparable detailed mapping was not available for the 1997-98 El Niño.

## 3. Observations

### 3.1. Sand Level Surveys

Surveys of subaerial beach sand levels from 1997-2014 at 5 beaches were obtained from several sources (Figure 1) including (1) cross-shore transects surveyed biannually from the back beach to ~8-10 m depth beginning in 1997 (San Diego Association of Governments (SANDAG); red transects in Figure 1) and (2) quarterly transects, beginning in 2004 (SIO; dense black, blue, or white transects in Figure 1) [*Yates et al.*, 2009a]. (3) Monthly subaerial shoreline parallel surveys beginning at Torrey Pines, and subsequently expanded to four additional sites (Imperial, Cardiff, Solana, and Camp Pendleton). (4) Airborne lidar in April 1998 (NASA's airborne topographic mapper (ATM); *Brock et al.*, [2002]) and biannually from May 2002 until October 2010 (Univ. of Texas, *Yates et al.*, [2008]). Lidar returns were removed offshore of the waterline location, estimated using water levels from a nearby tide gauge and runup approximated using local wave conditions [*Yates et al.*, 2008]. Lidar sand levels were gridded onto 4 $m^2$ cells, using the cell median elevation to reduce the influence of outliers. Point density in the 1998 NASA lidar survey was low (0.57 points $m^{-2}$), compared with the post-2001 biannual lidar surveys (~2 points $m^{-2}$) [*Brock et al.*, 2002;

*Yates et al.*, 2008]. Grid cells with less than 3 data points were discarded from the post-2001 lidar surveys. All data was necessarily retained in the lower density 1998 survey. Surveys from different sources at the same approximate time and beach usually agree, with differences owing to variable amounts of spatial averaging (Figure 3).

Responding to seasonal variations in wave energy, the observed shoreline (e.g. MSL contour) locations usually varied seasonally by 25-30 m at all 5 study beaches (Figure 4; [*Winant et al.*, 1975; *Yates et al.*, 2009b]). During the 1998 El Niño, shoreline retreat was maximal, about 25 m landward of the typical (e.g. 2004-2012) winter shoreline (Figure 4). Recovery from 1997-98 took several years, even with nourishments both shortly before (1997, Imperial Beach, 178,000 $m^3$) and after (1999, Solana Beach, 41,000 $m^3$) El Niño; however, during fall 1997, existing beach sand levels at several sites were historically lower than post-summer level observed in most other years. Accordingly, the erosive change during the 1997-98 El Niño was limited because of low sand levels preceding the event. Recovery following the less erosive 2009-10 El Niño was more rapid, effectively one season (Figures 3 and 4). Spring-summer 2001 nourishments at Imperial Beach, Torrey Pines, Solana Beach, and Cardiff elevated sand levels to new maxima (Figure 4). The nourishment was detectable for about two years at Torrey Pines, either as a wider subaerial beach, or as an enhanced offshore winter sand bar [*Yates et al.*, 2009c]. SANDAG winter surveys occur in spring and fall. The spring surveys usually occur after the winter erosion maximum in February-March (compare squares and circles in Figure 3a, in 2005-2008 inclusive), so the 1998 survey may not have captured the maximum erosion.

### 3.2. Waves

Waves typically approach the Southern California Bight from N-NW in winter and from S-SW in summer, and vary alongshore owing to sheltering by the Channel Islands and refraction over complex offshore bathymetry [*Pawka*,1983]. Local (e.g. < 30 m depth) bathymetric variations further refract and focus waves with appreciable alongshore energy variations over several hundreds meters alongshore. Directional wave buoys (CDIP, http://cdip.ucsd.edu; Figure 1a) initialized a spectral refraction model [*O'Reilly and Guza*, 1991, 1993, 1998] that provided hourly wave estimates at 10 m depth every 100 m alongshore. Near-shore buoy deployments confirmed reasonably good model accuracy in relatively shallow water (20-30 m depth) at several of the study sites [*Young et al., 2012*].

Waves were most energetic during strong El Niño winters (Figure 5a). For example, at the Oceanside buoy (Figure 1b), the hours of significant wave height $H_s$ exceeding 3 m were between 0-26 hours during 13 non-El Niño winters, compared with 40 and 51 hours in the 1997-98 and 2009-10 El Niño winters, respectively. Total hours of $H_s$ between 2-3 m during the 1997-98 El Niño winter (more than 400 hours) dwarfed all other winters, nearly doubling those found in the second most energetic winter (e.g. 2009-10 winter; 220 hours of $H_s$ = 2-3 m; Figure 5a). In 1997-98, $H_s$ exceeded 2 m for nearly 60 continuous hours, with frequent and prolonged sequences of energetic waves in early December 1997 and February 1998 (Figure 5b). January 2010 had the longest period (~ 140 hours) of continuous $H_s$ exceeding 2 m (Figure 5e).

## 4. Shoreline Modeling

### 4.1. Equilibrium Shoreline Model

An existing equilibrium shoreline model [*Y09*] was modified to improve predictions during El Niños and other severe erosion conditions by accounting for durable limits (e.g. bedrock, seawalls, hard cliffs). The model assumes these relatively resilient boundaries were not eroded during the modeling period, and neglects cliff erosion, which would both relocate the back beach boundary and supply new sand to the beach. The comparative beach profile effects between armored and exposed back beaches are not included in the present model. With the shoreline location $S$ defined as the cross-shore location of the MSL contour, the shoreline change rate $dS/dt$ depends on the present shoreline position $S$ and incident wave energy $E$,

$$\frac{dS}{dt} = \begin{cases} C^{\pm} E^{1/2} \Delta E(S) & \text{for } S > S_{bb} \\ 0 & \text{for } S \leq S_{bb} \end{cases} \tag{2a}$$

where $C^{\pm}$ are two change rate coefficients for accretion ($C^{+}$) and erosion ($C^{-}$), and the wave energy disequilibrium is

$$\Delta E(S) = E - E_{eq}(S). \tag{2b}$$

$E_{eq}$, the equilibrium wave energy, is the wave energy for a given $S$ that would cause no shoreline change . For the few occasions when highly accreted shoreline positions $S^{+}$ yielded non-physical negative $E_{eq}$ (e.g. $E_{eq}(S^{+}) < 0$), $E_{eq}(S^{+}) \equiv 0$, ensuring non-negative equilibrium wave energy. Unless otherwise noted, $E_{eq}$ is linearly related to the shoreline position $S$:

$$E_{eq}(S) = a_0 + a_1 S \quad (3)$$

where $a_0$ and $a_1$ are empirically determined equilibrium wave energy coefficients. New here, $S_{bb}$ is the non-erodible back beach cross-shore location defined using the aerial photographic and lidar surveys. Shoreline retreat stops (e.g. $dS/dt = 0$) when $S = S_{bb}$. A beach initially in equilibrium and subject to a step change in the incident wave energy equilibrates exponentially, with a characteristic e-folding time scale $\tau^{\pm} = \left| a_1 C^{\pm} \sqrt{E} \right|^{-1}$ [*Y09*].

Each beach was sub-divided into approximately 500 m alongshore sections, numbered from south to north within each site: I1-I9 (Imperial Beach), T1-T9 (Torrey Pines), S1-S5 (Solana Beach), C1-C4 (Cardiff), P1-P4 (Camp Pendleton). Incident wave energy, temporally-demeaned shoreline observations, and the back beach limit $S_{bb}$ (Figure 2) were alongshore averaged on transects within each 500 m section. Values of the model's four free parameters ($C^{+}, C^{-}, a_0, a_1$) were determined from these averaged shoreline observations and hourly wave estimates by minimizing the model-data root-mean-square error (RMSE) using surrogate management framework (SMF) optimization [*Booker et al.*, 1999; *Marsden et al.*, 2004].

**4.2. Model-Data Comparison**

Shorelines were hindcast for up to 16 years using the wave-driven equilibrium model, initialized with the earliest survey data point (typically fall 1997). Model calibration with a period including an El Niño yielded improved model-data agreement during both El Niño and non-El Niño years, and calibration with 2003-2011 is shown

(Figure 6). The average model skill at Solana, Imperial and Torrey Pines beaches are between 0.55-0.60 (Table 3). At Cardiff and Camp Pendleton, two shorter beaches with river or lagoon mouths, skill was often less than 0.5. Two of the four modeled sections at Cardiff have low skill (e.g. 0.22 and 0.41) and are located near a persistent lagoon mouth or a large bedrock platform extending from the subearial beach to wading depths. Camp Pendleton was observed for the shortest time, and has the lowest $R^2$ (less than 0.5 at all modeled sections; Figure 6e), possibly resulting from the adjacent river mouth. Skill at all modeled locations was significant at the 95% level.

The model back beach erosive limit $S_{bb}$ (Figure 2; dashed horizontal line in Figure 6a-d) was reached during the 1997-98 El Niño (except Camp Pendleton), and without the geological constraint the unmodified *Y09* model over-predicted erosion (red curve in Figure 6). $S_{bb}$ was reached only at a few sites in the 2009-10 El Niño. The maximum model beach width $S_{\max} = -a_0/a_1$ (positive horizontal dotted line in Figure 6) was exceeded a few times, usually after sand nourishments that are neglected in the model (e.g. accretion peaks in fall 1998 and fall 2001 at Imperial Beach (Figure 6a) and during summer-fall 2001 at Torrey Pines and Solana Beach (Figure 6b,c)). The anomalous accretive peak in summer 2006 at many of the sites is unexplained and not reproduced by the model.

## 5. Discussion

### 5.1. Parameter Values, Response Times, and Initialization

Optimal model free parameters varied within and between sites (Table 3). Model error is weakly sensitive to the free parameter values, with only a 10% increase in model error for factor of two of changes in parameters (comparable to the differences between sites). Free parameter values surely depend on sediment availability, grain size, and possibly other environmental factors, but are only loosely constrained by the observations.

The best-fit shoreline adjustment time scales $\tau^{\pm} = \left| a_1 C^{\pm} \sqrt{E} \right|^{-1}$, averaged over each site, varied between roughly 10-20 days for erosion $\tau^{-}$ (with $H_s = 4$ m), and the accretion $\tau^{+}$ spanned 29-64 days (with $H_s = 1$ m; Table 3). Hypothetical initial conditions illustrate the rapid return (weeks to several months) of the model to equilibrium from artificially large disequilibria (crosses and triangular markers in Figure 7). Six rather different initial conditions in 1996, 1997, and 1998 all result in the same modeled shoreline by summer 1998 (grey curve in Figure 7). Model shorelines recovered from strong 1997-98 El Niño erosion by the following winter, more rapid than the observed multi-year recovery, demonstrating the model's failure to properly replicate the slow return of sand evidently displaced further offshore during the strong event (Figures 6b-d). Accretion is crudely parameterized in the model and requires future study.

### 5.2. Calibration Period

At Torrey Pines, *Y09* found a relative 1.9 m increase in model-data RMSE during predictive model periods compared to the calibration period RMSE. *Splinter et al.* [2013] provide a more extensive calibration and validation discussion of a similar equilibrium-based 1-D shoreline model. Both Y09 and *Splinter et al.* [2013] showed that approximately two years of monthly observations suffice to calibrate empirical shoreline model parameters on seasonally variable beaches (Torrey Pines in southern California and along the eastern Australian coast). Here, three calibration periods are examined (Figure 8): 1997-2013 (all data; 16 years), 2003-2011 (8 years), and 2003-2008 (5 years). The 2003-2008 period lacks an El Niño. Model errors are characterized with the RMSE over 16 years, and with $\Delta_{W10}$, the difference between the maximum erosion observed and modeled during the 2009-10 El Niño winter. Solana Beach results weakly depended on calibration period (Figure 8, top). At the other sites, longer calibration periods that included an El Niño consistently decreased $\Delta_{W10}$ and RSME over the entire 16-year observation period, which included years of neutral and La Niña conditions (Figure 9a,b). The sparse 1997-2001 data were not well fit, even when 1997-2001 was included in the calibration (not shown). The 2003-2011 calibration period was used.

The alongshore variability of the 8-year calibration model coefficients was qualitatively similar to previous work [*Y09*] based on ~5 years of calibration that did not include El Niño (similar to the 2003-2008 calibration results in this study). Here, the relative magnitudes of the wave energy slope, $a_1$, and $C^{\pm}$ were reversed compared to *Y09* (e.g. *Y09* had larger (smaller) magnitude $a_1$ ($C^{\pm}$) compared to this study). These differences may be partially attributed to the increased calibration period, as longer tuning generally resulted in different free parameters and a reduction in RMSE [*Y09*]. However, direct comparison to the *Y09* results is cautioned, as modeled sections at the same beach are not necessarily identical to this study.

Additionally, the statistical nature of the calibration technique creates inherent variation to the resulting coefficients, as several solutions in parameter-space may produce similar results. The multiplicative nature of the model terms (2) also allows for changes in one coefficient to be compensated for by another coefficient.

Alongshore-averaged model coefficients provide a broad representation of the site-specific free-parameter value for bulk comparison to *Y09* (Table 3). Alongshore averaged, $C^{+}$ had the greatest disparity (more than double in magnitude) relative to *Y09* 5-year calibrated $C^{+}$ at Torrey Pines. However, as noted previously, model skill is fairly insensitive to parameter values, with $C^{+}$ being the least sensitive parameter [*Y09*]. Fundamentally, model coefficients are weakly constrained by observations and differences between studies, even at similar beaches, are not necessarily remarkable.

**5.3. Alternative Model Formulations**

*Davidson et al.* [2013] and *Splinter et al.* [2014] use an equilibrium model with forcing governed by wave power (rather than wave energy, $E$, in (2)) and the Dean parameter, which depends on grain size. The range of sand grain sizes is not taken into account here, and is relatively small (4 of the 5 beaches have $D_{50}$ between 0.15-0.18mm, (Table 1)). At Torrey Pines, *Y09* showed replacing wave energy, $E$, in their shoreline model with $H_s$ or radiation stress $S_{xx}$ resulted in similar model skill, because $E$, $H_s$, and $S_{xx}$ are strongly mutually correlated. *Davidson et al.* [2013] and others use an equilibrium condition based on the weighted average of antecedent waves, rather than on the present beach state. However, the present beach state depends on the previous wave conditions, and for the idealized case of a step change in time to a constant wave forcing, the equilibrium conditions of *Davidson et al.* [2013] and *Y09* yield identical results. These different equilibrium models were also shown to yield similar results for the field observations [*Castelle et al.*, 2014].

The basic equilibrium equation of the present model (2), with a linear dependence of $dS/dt$ on the present wave energy $E$, and 4 free parameters, is referred to as the linear$_4$ model (the subscript specifies the number of free parameters). Additional alternative models are linear$_3$, exp$_4$, and cubic$_4$. The linear$_3$ model reduces the number of free parameters to three by replacing $C^{\pm}$ with single valued $C$ in (2a), following *Yates et al.*, [2011]. The exp$_4$ and cubic$_4$ alternative models also simplify $C^{\pm}$ with $C$ in (2a), but use more complex forms of $E_{eq}$,

$$E_{eq} = a_0 e^{a_1(S-a_2)} \quad \text{for exp}_4 \tag{4}$$

and

$$E_{eq} = a_0 + a_1 S + a_2 S^3 \quad \text{for cubic}_4. \tag{5}$$

The model parameters $S_{eq}$ and $E_{eq}$, and the rate of change $dS/dt$ and the response time $\tau$, are similar in the range of common $S$ and $H_s$, while differing at the extremes (Figure 10). All models use the same erosion limiter $S_{bb}$.

Overall (2003-2011) the alternative models perform similarly, with typically small (<15%) improvements in model error relative to the *Y09* model, which has no erosion limiter (Figure 9c). Model performance varied by site, but explained more than 50% of the variance over 16 years at most of the sandy beaches, similar to *Y09* five-year hindcasts. The models differ from the *Y09* model most significantly for extreme conditions only briefly encountered. While the *Y09* model correctly identifies the 1997-98 waves as more erosive than 2009-10, it overestimates shoreline erosion during both El Niño events.

The $\text{cubic}_4$ model provided the greatest improvements in model skill (relative to *Y09*), with improved predictions for El Niño 2009-10 at beaches both where the erosion limiter was and was not reached (Solana Beach and Torrey Pines, respectively, Figure 9a,b). The over-prediction of the winter 2009-10 shoreline erosion ( $\Delta_{W10}$, Figure 9d) was reduced using the $\text{cubic}_4$ model at all sites except Camp Pendleton, where over-prediction persisted. Model-data comparison at Camp Pendleton was generally poor irrespective of which model was used, perhaps owing to the close proximity of a river mouth. Typical $\Delta_{W10}$ reductions are about 5 m (up to 18 m peak reduction) relative to *Y09*. With large waves ($H_s$ = 4 m) and a heavily eroded shoreline (solid curves, $S$ = -40 m, Figure 10d), $dS/dt$ for $\text{exp}_4$ and $\text{cubic}_4$ are much smaller in magnitude than for $\text{linear}_3$ (a simplified version of the *Y09* model). Physical explanations for the reduced mobility of eroded beach face include the exposure of resistant strata and/or a reduction of the effective wave energy reaching the beach face owing to well-developed offshore sandbars.

## 6. Conclusion

Sixteen years of shoreline and wave observations, including two El Niños, 1997-98 and 2009-10, illustrate seasonal and long-term fluctuations in wave climate and shoreline sand levels at five southern California beaches. An existing, empirical shoreline model driven with hourly wave conditions simulates well the seasonal changes in subaerial beach width (e.g. the cross-shore location of the MSL contour) during non-El

Niño years, similar to previous results [*Y09*]. During El Niño winters the *Y09* model over-prediction of shoreline erosion is reduced by including the location of erosion resistant boundaries (identified with aerial images), and using alternative, nonlinear forms of $E_{eq}$ (e.g. $cubic_4$) that gradually decrease the mobility of highly eroded shorelines (simulating cobbles, kelp wrack, enhanced offshore sand bars, and other stabilizing effects).

The shoreline location depends on complex processes occurring over the cross-shore beach profile, and in some cases on adjacent profiles. Even significantly different equilibrium shoreline models often have similar skill [*Castelle et al.*, 2014], which is also true for existing, more computationally demanding, physical process models for shoreline change. Application of any model to extreme conditions on sand-limited beaches with unknown substrates will requires site and condition specific calibration. Once trained, the present model provides a computationally simple (e.g. nonlinear first order differential equation) representation of the observed relationship between incident waves and shoreline change, including the effect of erosion resistant substrates.

## Acknowledgements

This research was supported by the United States Army Corps of Engineers and the California Department of Parks and Recreation Division of Boating and Waterways (program manager Reinhard Flick). The paper was substantially improved by reviewer and editor commments. André Doria was supported by Fellowships from the University of California Regents, NDSEG, and the National Science Foundation (GRFP).
SANDAG, Coastal Frontiers Corporation, and Fugro are thanked for their assistance in

using their datasets. This publication was prepared by André Doria under NOAA Grant #NA10OAR4170060. California Sea Grant Project R/RCC-01, through NOAA's National Sea Grant College Program and the U.S. Dept. of Commerce. The statements, findings, conclusions and recommendations are those of the author(s) and do not necessarily reflect the views of the aforementioned organizations.

## References

Allan, J. C., and P. D. Komar (2002), Extreme storms on the Pacific Northwest Coast during the 1997–98 El Niño and 1998–99 La Niña, J. Coastal Res., 18(1), 175–193.

Allan, J. C., and P. D. Komar (2006), Climate controls on US West Coast erosion processes, J. Coastal Res., 22(3), 511–529, doi:10.2112/03- 0108.1.

Bamber, Jonathan L., Riccardo E. M. Riva, Bert L. A. Vermeersen, Anne M. LeBrocq (2009), Reassessment of the Potential Sea-Level Rise from a Collapse of the West Antarctic Ice Sheet, Science, 324(5929), 901-903, doi: 10.1126/science.1169335

Barnard, P. L., J. Allan, J. E. Hansen, G. M. Kaminsky, P. Ruggiero, and A. Doria (2011), The impact of the 2009–10 El Niño Modoki on U.S. West Coast beaches, Geophys. Res. Lett., 38(13), doi:10.1029/2011GL047707.

Booker, A. J., J. E. Inman, P. D. Frank, D. B. Serafini, V. Torczon, and M. W. Trosset (1999), A rigorous framework for optimization of expensive functions by surrogates, Struct. Multidiscip. Optim., 17(1), 1–13.

Brock, J.C., C. Wayne Wright, Asbury H. Sallenger, William B. Krabill and Robert N. Swift (2002), Basis and Methods of NASA Airborne Topographic Mapper Lidar Surveys for Coastal Studies, J. Coastal Res., 18(1), 1-13.

California Department of Boating and Waterways and State Coastal Conservancy (2002), California Beach Restoration Study, Sacramento, California Department of Boating and Waterways and State Coastal Conservancy, Sacramento, Cali., http://www.dbw.ca.gov/PDF/Reports/BeachReport/FUll.pdf.

Castelle, Bruno, Vincent Marieu, Stéphane Bujan, Sophie Ferreira, Jean-Paul Parisot, Sylvain Capo, Nadia Sénéchal, and Thomas Chouzenoux (2014), Equilibrium shoreline modelling of a high-energy meso-macrotidal multiple-barred beach, Marine Geology, 347, 85–94, doi:10.1016/j.margeo.2013.11.003.

Coastal Frontiers Corporation (2002), SANDAG 2001 Regional Beach Monitoring Program annual report, Coastal Frontiers Corporation, Chatsworth, Cali., http://www.sandag.org/uploads/projectid/projectid_101_16641.pdf.

Davidson, M.A., R.P. Lewis, and I.L. Turner (2010), Forecasting seasonal to multi-year shoreline change, Coastal Engineering, 57(6), 620-629, doi:10.1016/j.coastaleng.2010.02.001.

Davidson, M.A., K.D. Splinter, and I.L. Turner (2013), A simple equilibrium model for predicting shoreline change, Coastal Engineering, 73, 191–202, doi:10.1016/j.coastaleng.2012.11.002

Dyurgerov, Mark B., and Mark F. Meier (2000), Twentieth century climate change: Evidence from small glaciers, Proceedings of the National Academy of Sciences, 97(4), 1406-1411.

Flick, Reinhard E., and B.Walton Waldorf (1984), Performance documentation of the Longard Tube at Del Mar, California 1980–1983, Coastal Engineering, 8(3), 199-217, doi:10.1016/0378-3839(84)90001-2.

Gallien, T.W., J.E. Schubert, and B.F. Sanders (2011), Predicting tidal flooding of urbanized embayments: A modeling framework and data requirements, Coastal Engineering, 58(6), 567-577, doi:10.1016/j.coastaleng.2011.01.011.

Graham, N. E., and H. F. Diaz (2001), Evidence for intensification of North Pacific winter cyclones since 1948, Bull. Am. Meteorol. Soc., 82, 1869–1893, doi:http://dx.doi.org/10.1175/1520-0477(2001)082<1869:EFIONP>2.3. CO;2.

Johnson, Bradley D., Nobuhisa Kobayashi, and Mark B. Gravens (2012), Cross-Shore Numerical Model CSHORE for Waves, Currents, Sediment Transport and Beach Profile, ERDC/CHL TR-12-22, Coastal and Hydraulics Lab. (U.S.) Eng. Res. and Dev. Center (U.S.), Vicksburg, Miss.

Keeling, C. D., T. P. Whorf, M. Wahlen, and J. Van Der Plichtt (1995), Nature, 375, 666-670, doi: 10.1038/375666a0.

Larson, M., and N. C. Kraus (1989), SBEACH: Numerical model for simulating storm-induced beach change, Tech. Rep. CERC-89-9, U.S. Army Corps of Eng., Vicksburg, Miss.

Ludka, B. C., R. T. Guza, W. C. O'Reilly, and M. L. Yates (2015), Field Evidence of Beach Profile Evolution Towards Equilibrium, J. Geophys. Res. Oceans, 120, doi:10.1002/2015JC010893.

Marsden, A. L., M. Wang, J. E. Dennis, and P. Moin (2004), Optimal aerocoustic shape design using the surrogate management framework, Optim. Eng., 5(2), 235–262.

McLachlan, A., and A. Brown (2010), The Ecology of Sandy Shores, Academic Press, Burlington, Mass.

Miller, Jon K., and Robert G. Dean (2004), A simple new shoreline change model, Coastal Eng., 51(7), 531–556, doi:10.1016/j.coastaleng.2004.05.006.

Moore, L.J., B.T. Benumof, and G. B. Griggs (1999), Coastal erosion hazards in Santa Cruz and San Diego Counties, California, J. Coastal Res., SI(28), 121-139.

Nordstrom, C. E., and D. L. Inman (1975), Sand level changes on Torrey Pines Beach, California, (U.S.) Coastal Eng. Res. Center, Fort Belvoir, Virg.

O'Reilly, W.C. and R.T. Guza (1991), Comparison of spectral refraction and refraction-diffraction wave models, J. Waterway, Port, Coastal, and Ocean Engineering, 117, 199-215.

O'Reilly, W.C., and R.T. Guza (1993), A comparison of spectral wave models in the Southern California Bight, Coastal Eng., 19, 263-282.

O'Reilly, W.C., and R.T. Guza (1998), Assimilating coastal wave observations into regional swell predictions. Part I: Inverse methods, J. Phys. Oceanogr., 28, 679-691.

Pawka, S. S. (1983), Island shadows in wave directional spectra, J. Geophys. Res., 88(C4), 2579–2591, doi:10.1029/JC088iC04p02579.

Pfeffer, W. T., J. T. Harper, and S. O'Neel (2008), Kinematic constraints on glacier contributions to 21st- century sea- level rise, Science, 321, 1340–1343, doi:10.1126/science.1159099.

Rahmstorf, Stefan, Anny Cazenave, John A. Church, James E. Hansen, Ralph F. Keeling, David E. Parker, and Richard C. J. Somerville (2007), Recent Climate Observations Compared to Projections, Science, 316, doi: 10.1126/science.1136843.

Revell, David L., Paul D. Komar, and Asbury H. Sallenger Jr. (2002), An Application of LIDAR to Analyses of El Niño Erosion in the Netarts Littoral Cell, Oregon, J. Coastal Res., 18(4), 792-801.

Revell, David L., Jenifer E. Dugan, and David M. Hubbard (2011), Physical and Ecological Responses of Sandy Beaches to the 1997–98 El Niño, J. Coastal Res. 27(4), 718 – 730, doi:http://dx.doi.org/10.2112/JCOASTRES-D-09-00179.1.

Roelvink, Dano, Ad Reniers, Ap van Dongeren, Jaap van Thiel de Vries, Robert McCall, and Jamie Lescinski (2009), Modelling storm impacts on beaches, dunes and barrier islands, Coastal Eng., 56, 1133-1152, doi:10.1016/j.coastaleng.2009.08.006.

Ruggiero, Peter, P. D. Komar, and J. C. Allan (2010a), Increasing wave heights and extreme- value projections: The wave climate of the U.S. Pacific Northwest, Coastal Eng., 57, 539–552, doi:10.1016/j.coastaleng. 2009.12.005.

Ruggiero, Peter, Maarten Buijsman, George M. Kaminsky, and Guy Gelfenbaum (2010b), Modeling the effects of wave climate and sediment supply variability on large-scale shoreline change, Marine Geology, 273, 127-140.

Shepard, F.P. (1950), Beach cycles in southern California, Tech. Memo 20, Beach Erosion Board, U.S. Army Corps of Engineers, Washington, D.C.

Splinter, K.D., I. L. Turner, and M. A. Davidson (2013), How much data is enough? The importance of morphological sampling interval and duration for calibration of empirical shoreline models, Coastal Eng., 77, 14-27, doi:10.1016/j.coastaleng.2013.02.009.

Splinter, K. D., I. L. Turner, M. A. Davidson, P. Barnard, B. Castelle, and J. Oltman-Shay (2014), A generalized equilibrium model for predicting daily to interannual shoreline response, J. Geophys. Res., 119, 1936–1958, doi:10.1002/2014JF003106.

Vermeer, M., and S. Rahmstorf (2009), Global sea level linked to global temperature, Proc. Natl. Acad. Sci. U. S. A., 106(51), 21527-21532, doi:10.1073/pnas.0907765106.

Warrick, J.A., K. Rosenberger, A. Lam, J. Ferreira, I. M. Miller, M. Rippy, J. Svejkovsky, and N. Mustain (2012), Observations of coastal sediment dynamics of the Tijuana Estuary Fine Sediment Fate and Transport Demonstration Project, Imperial Beach, California, U.S. Geological Survey, Open-File Report 2012–1083, http://pubs.usgs.gov/of/2012/1083/.

Winant, C. D., D. L. Inman, and C. E. Nordstrom (1975), Description of seasonal beach changes using empirical eigenfunctions, J. Geophys. Res., 80, 1979–1986.

Wright, L.D, A.D Short, and M.O Green (1985), Short-term changes in the morphodynamic states of beaches and surf zones: An empirical predictive model, Marine Geology, 62, 339-364, doi:10.1016/0025-3227(85)90123-9.

Yang, B., M. Madden, J. Kim, and T. R. Jordan (2012), Geospatial analysis of barrier island beach availability to tourists. Tourism Manage., 33, 840–854.

Yates, M.L., R. T. Guza, Roberto Gutierrez, and Richard Seymour (2008), A Technique for Eliminating Water Returns from Lidar Beach Elevation Surveys, J. Atmos. Oceanic Technol., 25, 1671–1682, doi:10.1175/2008JTECHO561.1.

Yates, M. L., R. T. Guza, and W. C. O'Reilly (2009a), Equilibrium shoreline response: Observations and modeling, J. Geophys. Res., 114, doi:10.1029/2009JC005359.

Yates, M. L., R. T. Guza, W. C. O’Reilly, and R. J. Seymour (2009b), Overview of seasonal sand level changes on Southern California beaches, Shore & Beach, 77, 39–46.

Yates, M. L., R. T. Guza, W. C. O’Reilly, and R. J. Seymour (2009c), Seasonal persistence of a small southern California beach fill, Coastal Eng., 56, 559-564, doi:10.1016/j.coastaleng.2008.11.004.

Yates, M. L., R. T. Guza, W. C. O’Reilly, J.E. Hansen, and P. L. Barnard (2011), Equilibrium shoreline response of a high wave energy beach, J. Geophys. Res., 116, doi: 10.1029/2010JC006681.

Young, A. P., J. H. Raymond, J. Sorenson, E. A. Johnstone, N. W. Driscoll, R. E. Flick, and R. T. Guza (2010), Coarse sediment yields from seacliff erosion in the Oceanside Littoral Cell. Journal of Coastal Research, 26(3), 580–585.

Young, A. P., R. T. Guza, P. N. Adams, W. C. O'Reilly, and R. E. Flick (2012), Cross-shore decay of cliff top ground motions driven by local ocean swell and infragravity waves, J. Geophys. Res., 117, doi:10.1029/2012JC007908.

Zhang, Keqi, Bruce C. Douglas, and Stephen P. Leatherman (2004), Global warming and coastal erosion, Climatic Change, 64, 41-58.

## Tables

**Table 1.** Beach Alongshore Distance, Beach Facing Azimuthal Direction, Median Sand Grain Diameter ($D_{50}$), Beach Slope at MSL, MSL Minimum, Maximum, and Standard Deviation Horizontal Displacement from Average MSL Location, Number of Surveys, and Survey Date Range for Each Site.

| Site | Alongshore Distance (km) | Direction (deg) | $D_{50}$ (mm) | Beach Slope | MSL min/max ($\sigma$) (m) | Number of Surveys | Date Range |
|---|---|---|---|---|---|---|---|
| Imperial Beach | 4 | 250-270 | 0.28[a] | 0.02-0.05 | -23.6/25.8 (10.5) | 97 | Oct 1997-Aug 2012 |
| Torrey Pines | 8 | 260-270 | 0.15[b] | 0.01-0.08 | -31.5/26.2 (9.1) | 226 | Oct 1997-Jan 2014 |
| Solana Beach | 2.6 | 240-265 | 0.15[b] | 0.02-0.08 | -22.5/20.5 (7.6) | 103 | Oct 1997-Aug 2012 |
| Cardiff | 2 | 260 | 0.15[b] | 0.02-0.11 | -27.3/22.8 (9.5) | 136 | Oct 1997-Aug 2012 |
| Camp Pendleton | 2.5 | 235 | 0.18[b] | 0.02-0.04 | -35.8/19.4 (9.7) | 72 | Oct 1998-Oct 2010 |

[a]Collected May 2008 in the swash zone [*Warrick et al.*, 2012].
[b]Collected spring 2006 near the high tide line [*Yates et al.*, 2009b].

**Table 2.** Historical Beach Nourishment Placement Dates, Receiver Sites, Qualitative Placement Locations, Nourishment Volumes, Nourishment Pad Approximate Length and Width, and Nourishment Sand Median Grain Diameter ($D_{50}$).

| Placement Date | Receiver Site | Placement Location | Volume ($10^3$ $m^3$) | Length (m) | Width (m) | $D_{50}$ (mm) |
|---|---|---|---|---|---|---|
| 1995 | Imperial Beach | Near-shore[a] | 31.3 | - | - | - |
| 1996 | Imperial Beach | Near-shore[a] | 35.9 | - | - | - |
| 1997 | Imperial Beach | Subaerial Beach[b] | 13.7 | - | - | - |
| 1997 | Imperial Beach | Near-shore[a] | 178.1 | - | - | - |
| 1999 | Solana Beach | Subaerial Beach | 41.2 | - | - | - |
| 6-27 April, 2001 | Torrey Pines | Subaerial Beach | 187.3 | 488 | 49 | 0.14 |
| 22 May-4 June, 2001 | Imperial Beach | Subaerial Beach | 91.7 | 701 | 37 | 0.24-0.52 |
| 15-24 June, 2001 | Solana Beach | Subaerial Beach | 111.6 | 579 | 21 | 0.14 |
| 2-10 August, 2001 | Cardiff | Subaerial Beach | 77.2 | 274 | 46 | 0.34 |

[a]Placed in near-shore depths beneath the water surface.
[b]Placed south of the Tijuana River Mouth.
[*Coastal Frontiers Corporation*, 2002; *California Department of Boating and Waterways and State Coastal Conservancy*, 2002]

**Table 3.** Alongshore averages and standard deviations of optimal model free parameters and $R^2$ at each site. Average characteristic adjustment timescales[a] $\tau^{\pm}$ are shown in parenthesis and have units of days. The calibration period is October 2003-October 2011. $R^2$ is for model runs over all available data.

| | $a_1$ $(10^{-3}\,\mathrm{m}^2/\mathrm{m})$ | $C^-$ $(\mathrm{mh}^{-1}/\mathrm{m}^3)$ | $C^+$ $(\mathrm{mh}^{-1}/\mathrm{m}^3)$ | $a_1C^-$ $(\tau^-)$ $(10^{-3}\ \mathrm{m}^{-1}\mathrm{h}^{-1})$ | $a_1C^+$ $(\tau^+)$ $(10^{-3}\ \mathrm{m}^{-1}\mathrm{h}^{-1})$ | $R^2$ |
|---|---|---|---|---|---|---|
| Imperial Beach | -4.5±1.7 | -0.92±0.72 | -1.06±0.94 | 3.5±2.5 (21) | 3.6±2.4 (64) | 0.55±0.13 |
| Torrey Pines | -2.2±0.9 | -3.90±2.67 | -4.58±2.02 | 6.6±3.2 (9) | 10.3±5.7 (29) | 0.58±0.08 |
| Solana Beach | -5.8±2.5 | -1.26±0.67 | -0.83±0.43 | 7.6±3.5 (21) | 4.0±1.7 (54) | 0.60±0.08 |
| Cardiff | -5.4±3.1 | -2.16±1.52 | -1.49±1.92 | 14.3±16.9 (14) | 4.7±4.1 (57) | 0.43±0.15 |
| Camp Pendleton | -5.9±2.3 | -0.62±0.10 | -0.79±0.13 | 3.5±0.8 (12) | 4.8±2.5 (41) | 0.38±0.03 |

[a] $H_s = 4$ m (1 m) was used for estimating $\tau^-$ ($\tau^+$).

**Figures**

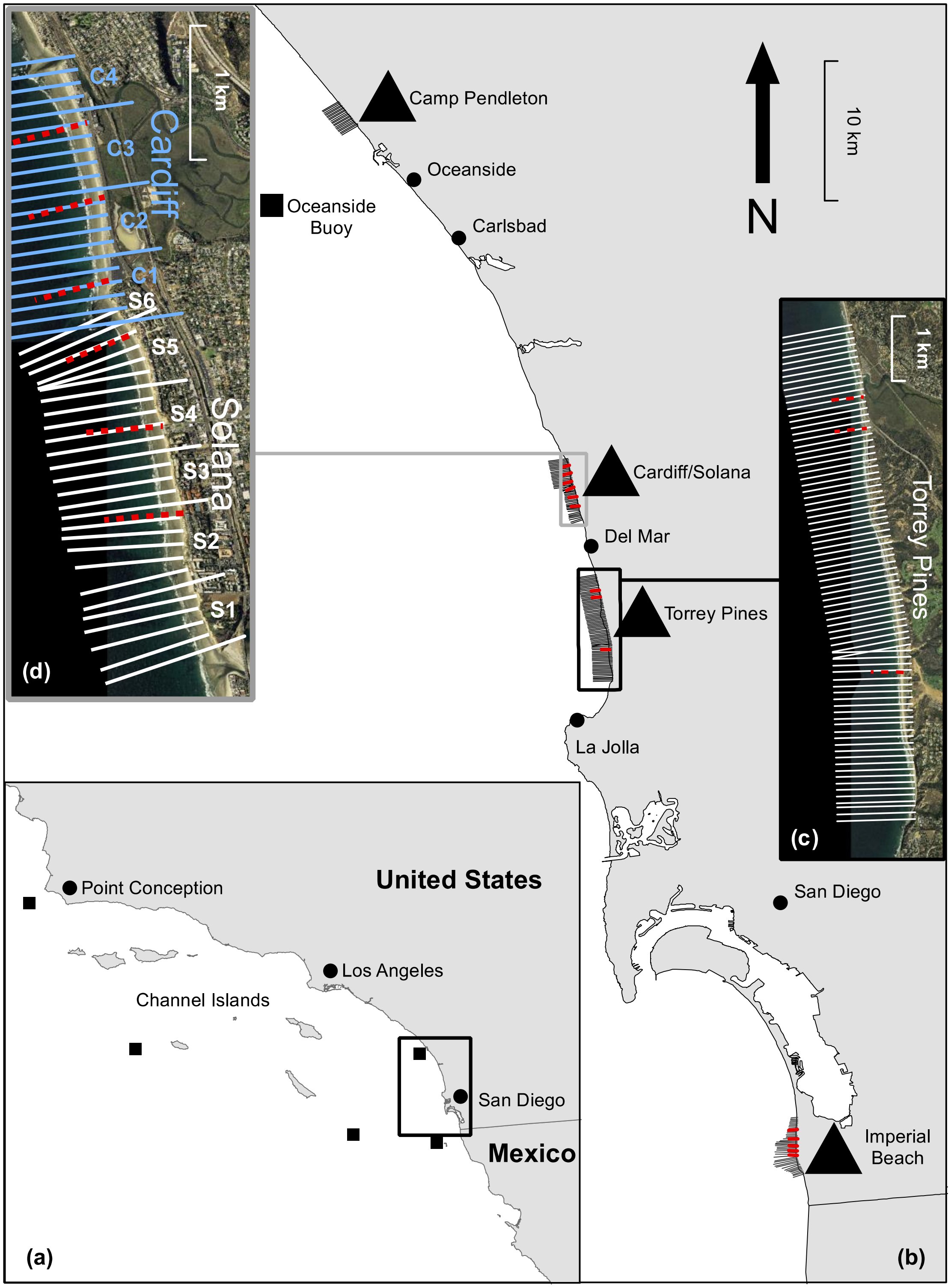

Camp Pendleton
Oceanside
Carlsbad
Oceanside Buoy
N
10 km
Cardiff/Solana
Del Mar
Torrey Pines
La Jolla
San Diego
Imperial Beach
(b)
1 km
Torrey Pines
(c)
1 km
C4
C3
Cardiff
C2
C1
S6
S5
S4
Solana
S3
S2
S1
(d)
Point Conception
United States
Los Angeles
Channel Islands
San Diego
Mexico
(a)

**Figure 1.** (a) Southern California map with wave buoy locations (black squares). (b) San Diego area map with study beaches (black triangles), near-shore buoy (black square), and survey transects (black (red) lines are SIO (SANDAG) transects). (c) Torrey Pines and (d) Solana Beach and Cardiff plan views. Cross-shore transects of SIO quarterly surveys (January, April, July, October) are white and blue lines, and SANDAG biannual (May, October) are red lines. For model comparisons, surveys were alongshore averaged in 500 m segments, labeled in (d).

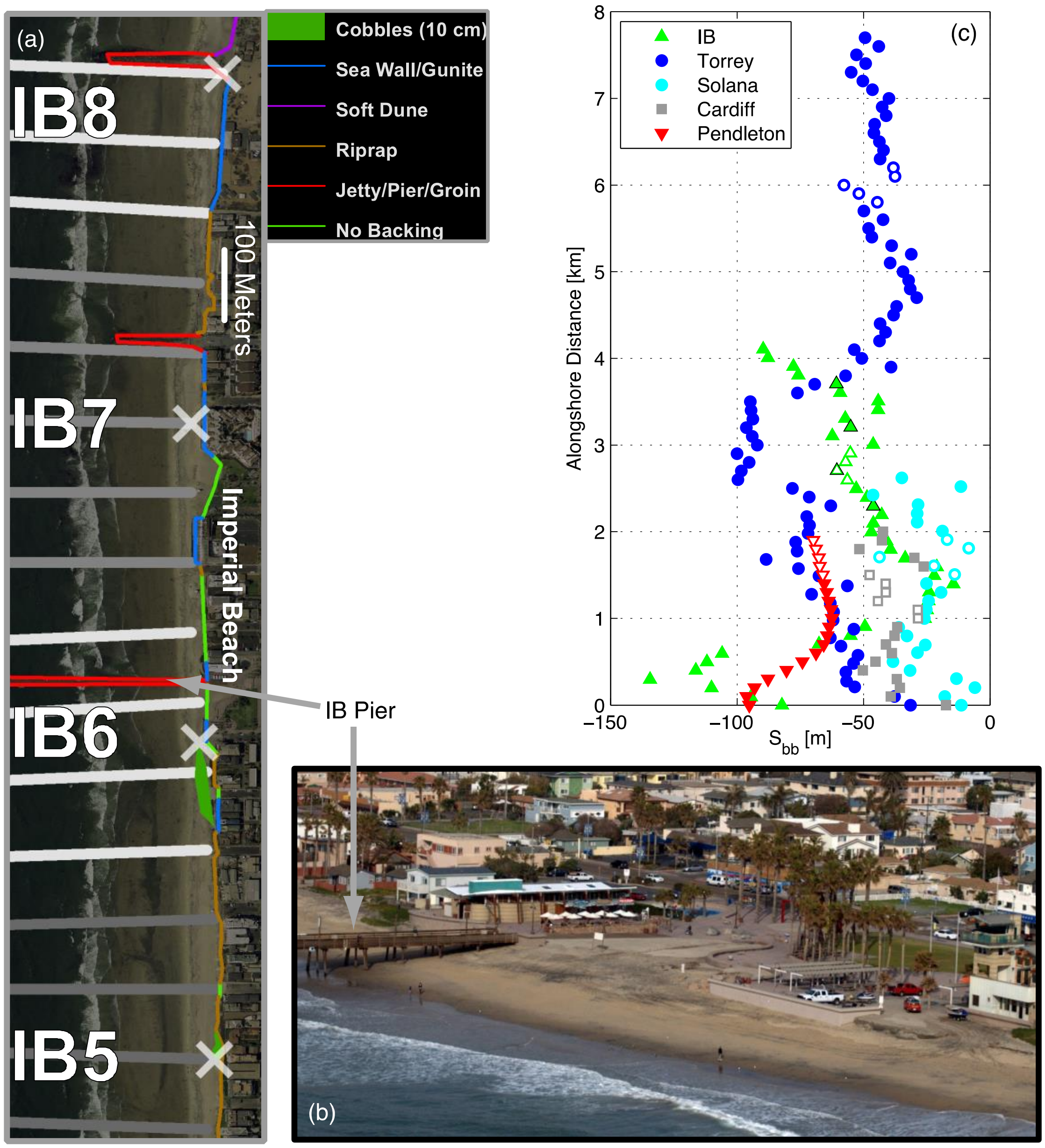


**Figure 2.** (a) Aerial image of Imperial Beach with subaerial substrate and back beach types (legend). Cross-shore survey transects, spaced 100 m alongshore, are averaged over approximately 500 m alongshore sections for modeling (IB5-IB8; (a) centers marked with white crosses). Transects within model section are indicated by alternating white and gray transect shadowing (end sections have additional transects outside of frame (a)). (b) Helicopter-based image of Imperial Beach (section IB6; February 2010).

Imperial Beach Pier in (a) and (b) is indicated with gray arrows. (c) The non-erodible shoreward boundary cross-shore location $S_{bb}$ (referenced to the average shoreline (MSL) location; negative is shoreward) on each transect versus alongshore distance for all five beaches. $S_{bb} \approx$ -58 m for the heavily cobbled backbeach in section IB6 (alongshore distance 2.6-2.9 km). Location of 500 m modeled sections, for each beach in Figure 6, are indicated by markers with white centers in (c), and black edged triangles in (c) correspond to locations of transects nearest to white crosses in (a).

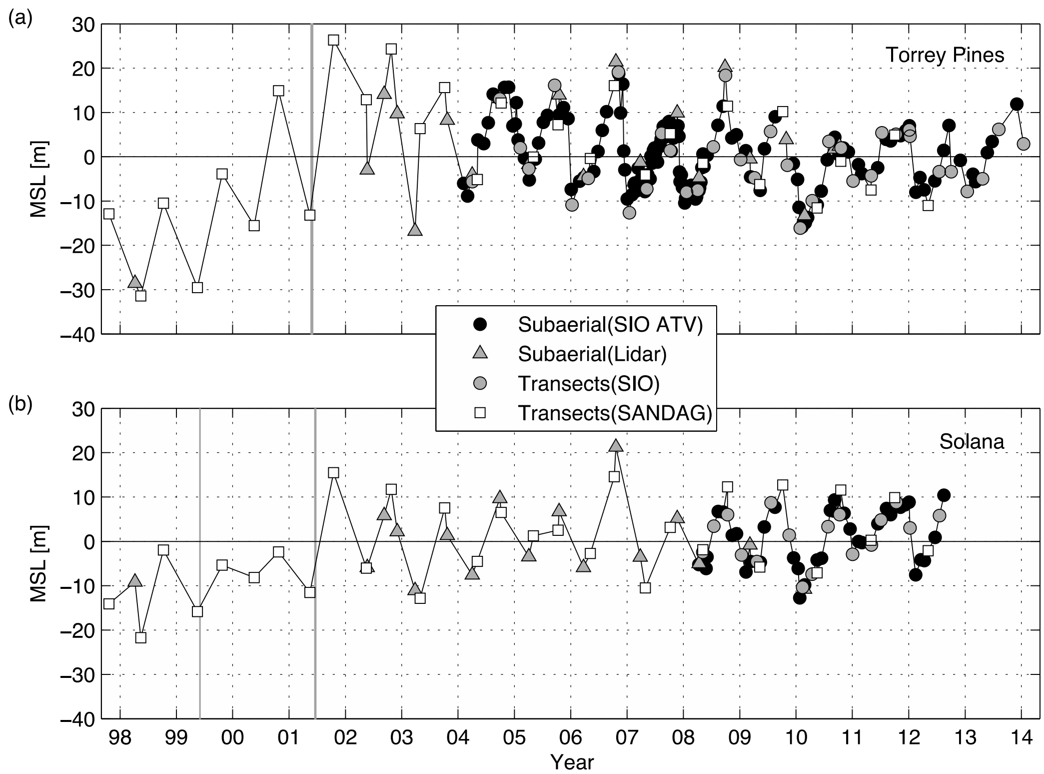


**Figure 3.** MSL cross-shore position (demeaned and alongshore averaged) versus time (tics are 1 January) for 16 years at (a) Torrey Pines and (b) Solana Beach. All available transects of each survey (legend indicates survey type, see Figure 1) are averaged. Positive (negative) values correspond to a wide (narrow) subaerial beach. Vertical gray lines indicate beach nourishment periods.

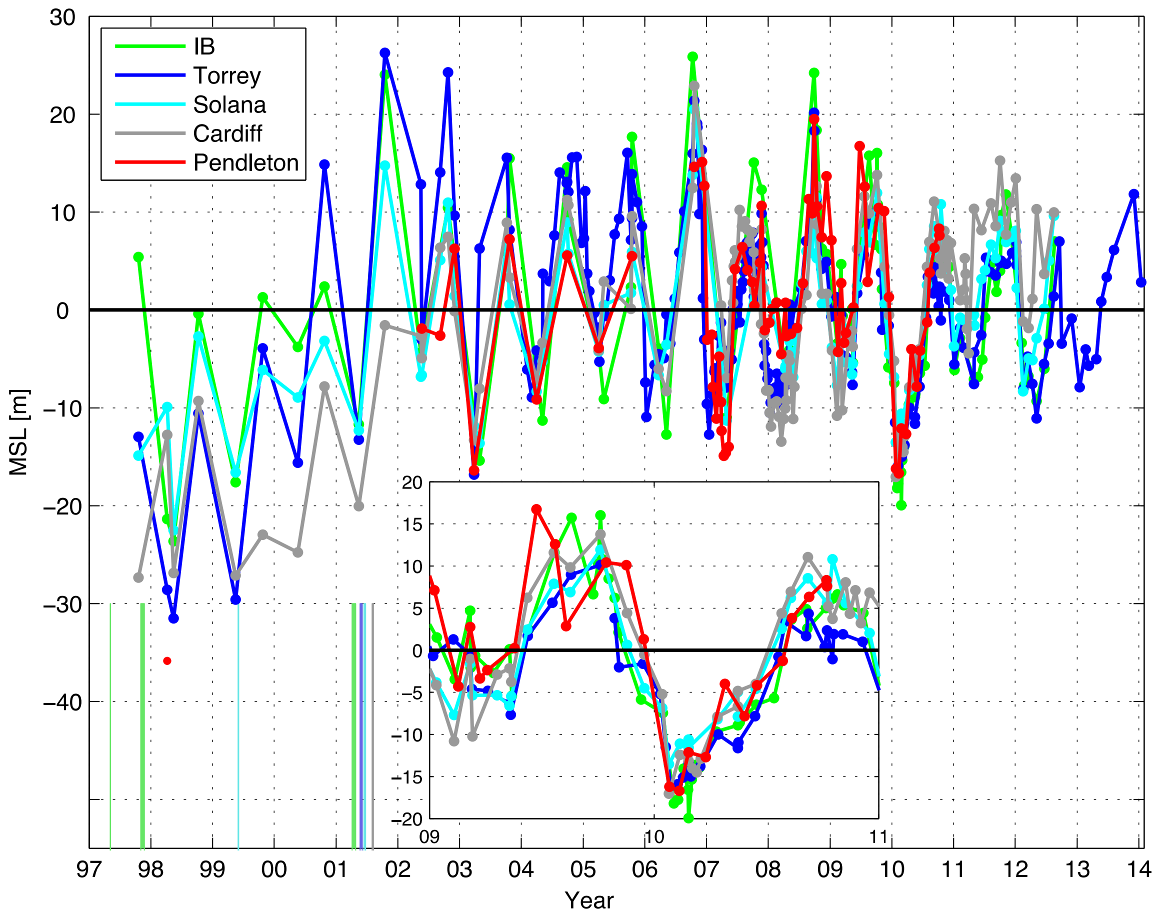


**Figure 4.** MSL cross-shore position (demeaned and alongshore averaged) versus time (tics are 1 January) for 16 years at 5 sites (see legend) from all data sources. Shortened colored vertical lines (see legend) indicate beach nourishment periods. Inset expands the 2009-10 El Niño winter.

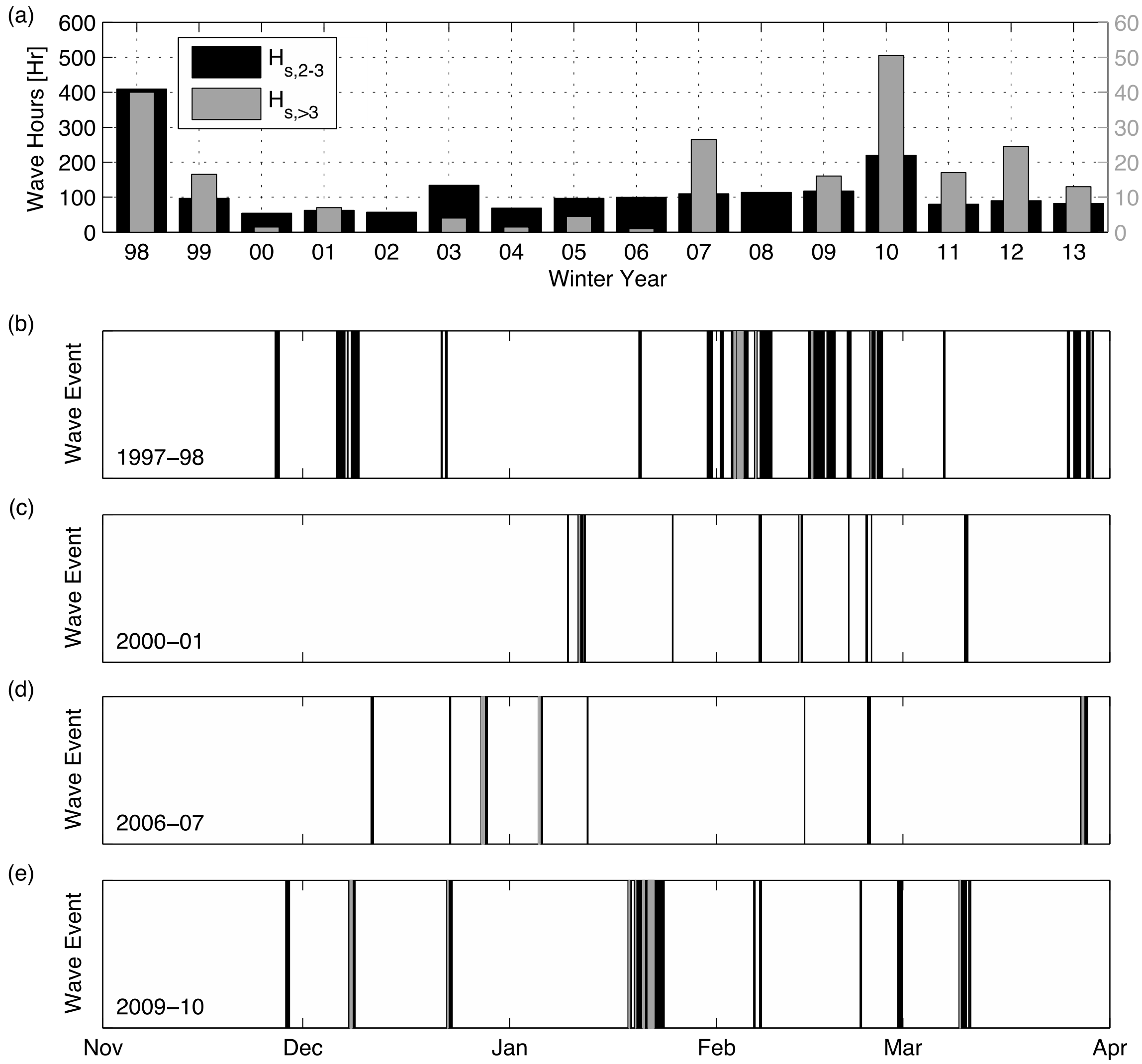


**Figure 5.** (a) Hours of observed $H_s$ between 2-3 m, and greater than 3 m (see legend) versus winter year (November-March) from November 1997 through March 2013 at Oceanside Buoy (Figure 1). Temporal occurrences of wave events within $H_s$ ranges (legend) for winters (b) 1997-98 (El Niño), (c) 2000-01, (d) 2006-07, and (e) 2009-10 (El Niño)

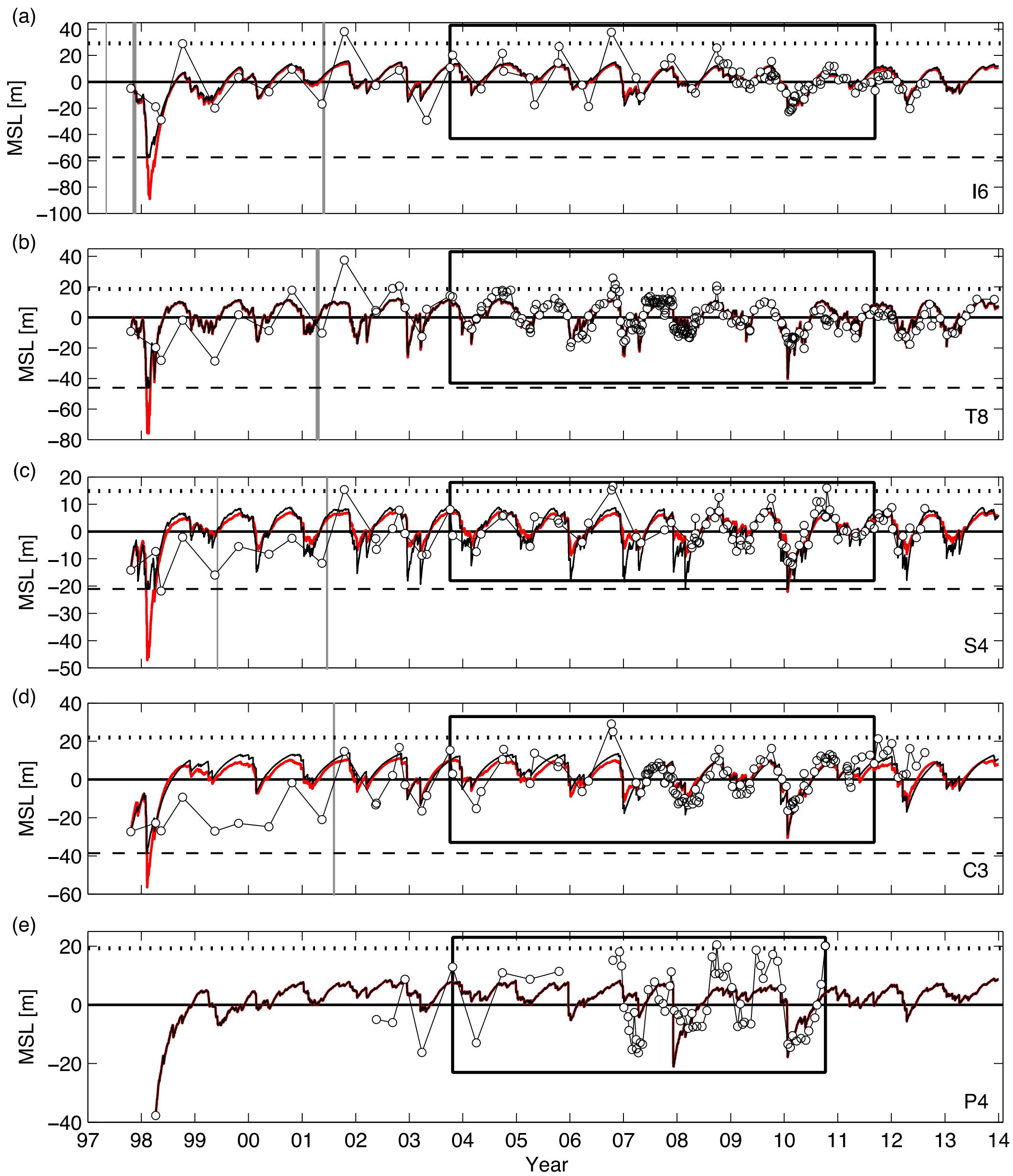


**Figure 6.** MSL position versus time (tics are 1 January) for representative 500 m long sections at (a) Imperial Beach (section I6) and (b) Torrey Pines (T8), (c) Solana Beach (S4), (d) Cardiff (C3), and (e) Camp Pendleton (P4). Shoreline observations are white circles. Model predictions (linear$_4$ model, black curve; *Y09* model, red curve) differ primarily in 1997-98. Model calibration period (black rectangle), non-erodible back beach limit $S_{bb}$ (dashed horizontal black line), fully equilibrated shoreline $S = -a_0/a_1$

for $E = 0$ (dotted horizontal black line), and beach nourishments (vertical gray bands) are shown. Model root-mean-square errors ($R^2$) over 16-years are (a) 8.6 m (0.57), (b) 6.3 m (0.65), (c) 5.2 m (0.52), (d) 8.9 m (0.41), and (e) 8.8 m (0.43).

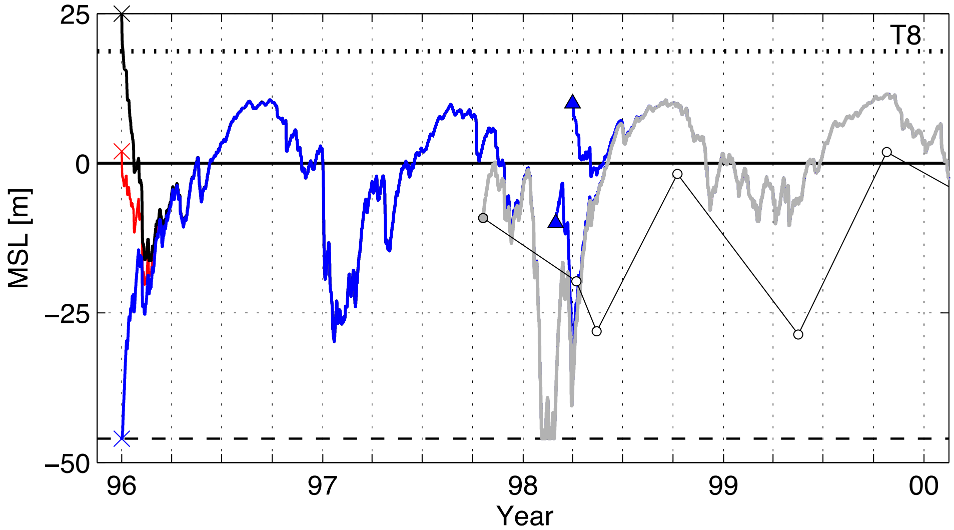


**Figure 7.** Modeled MSL position versus time at Torrey Pines (section T8, calibrated with 2003-2011 data) with different initial conditions. January 1996 with three hypothetical MSL shorelines (~0, 25 and -50 m; colored crosses) yield colored curves that rapidly converge together. Fall 1997 was initialized with the observed shoreline (gray circle and curve) and spring 1998 was initialized with ±10 m (two black-blue triangles). By summer 1998, all 6 model initializations yield the same result (gray curve). Horizontal lines are non-erodible back beach $S_{bb}$ (dashed) and fully accreted beach (dotted), $S = -a_0/a_1$.

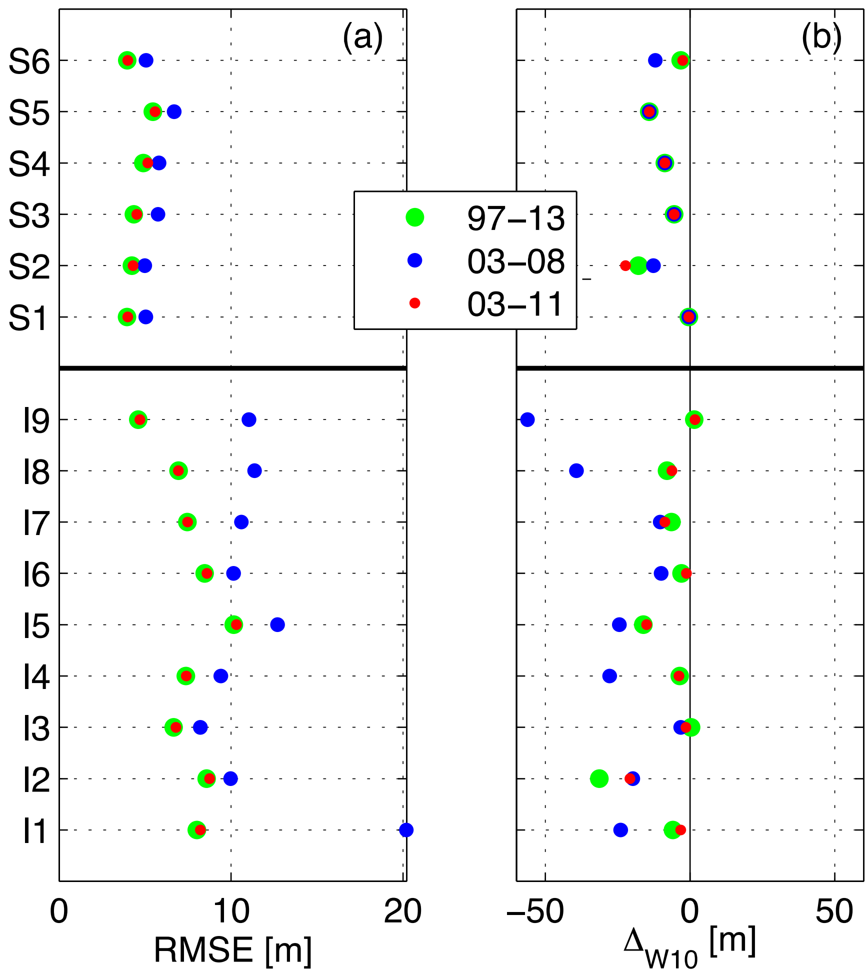


**Figure 8.** Model (linear$_4$) (a) RMSE (all data) and (b) model-data winter (January-March) 2010 erosion minimum error versus each 500 m alongshore section at Solana Beach (top, sections S1-S6) and Imperial Beach (bottom, I1-I9) for three model calibration periods. (b) Negative values indicate model over-predicts erosion minimum.

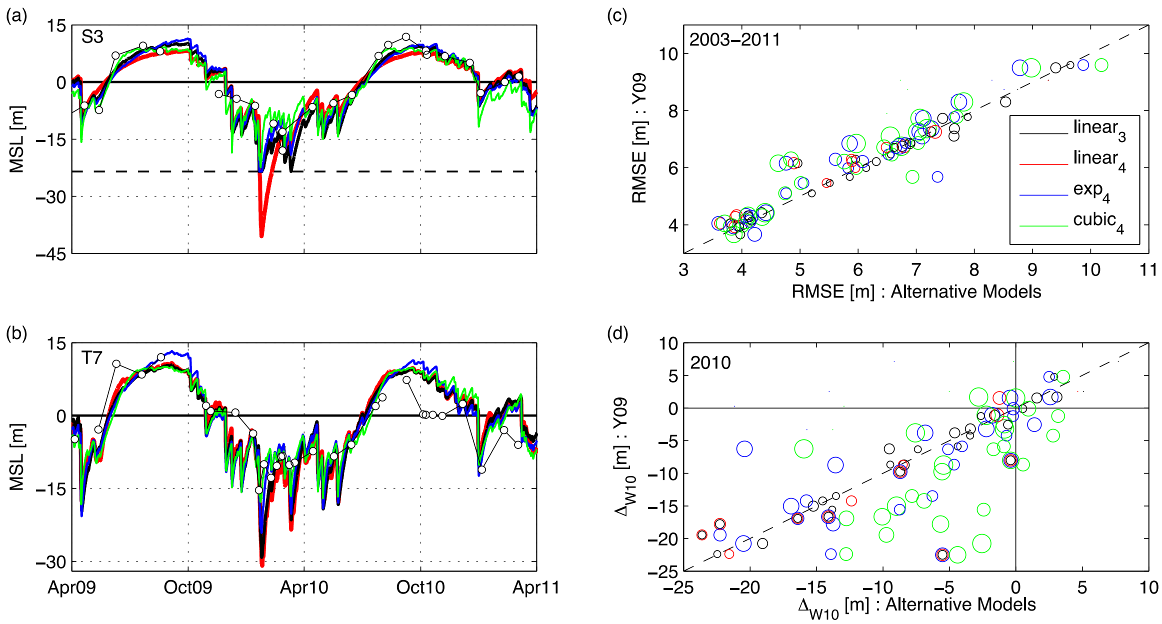


**Figure 9.** Modeled and observed (white circles) MSL versus time at (a) Solana Beach (section S3) and (b) Torrey Pines (T7). (a) Dashed black horizontal line indicates $S_{bb}$, the non-erodible back beach limit. Red curve in (a) and (b) is the *Yates et al.* [2009a] (unrestricted linear$_4$) model (e.g. *Y09* model). Note vertical scales differ in (a) and (b). (c) RMSE (October 2003-October 2011) and (d) model-data winter 2010 (January-March 2010) erosion minimum error for the *Y09* model (vertical axis) versus alternative models. In panels (c) and (d), symbol size varies for visibility. (a-d) Model types are indicated by colors (legend in (c)).

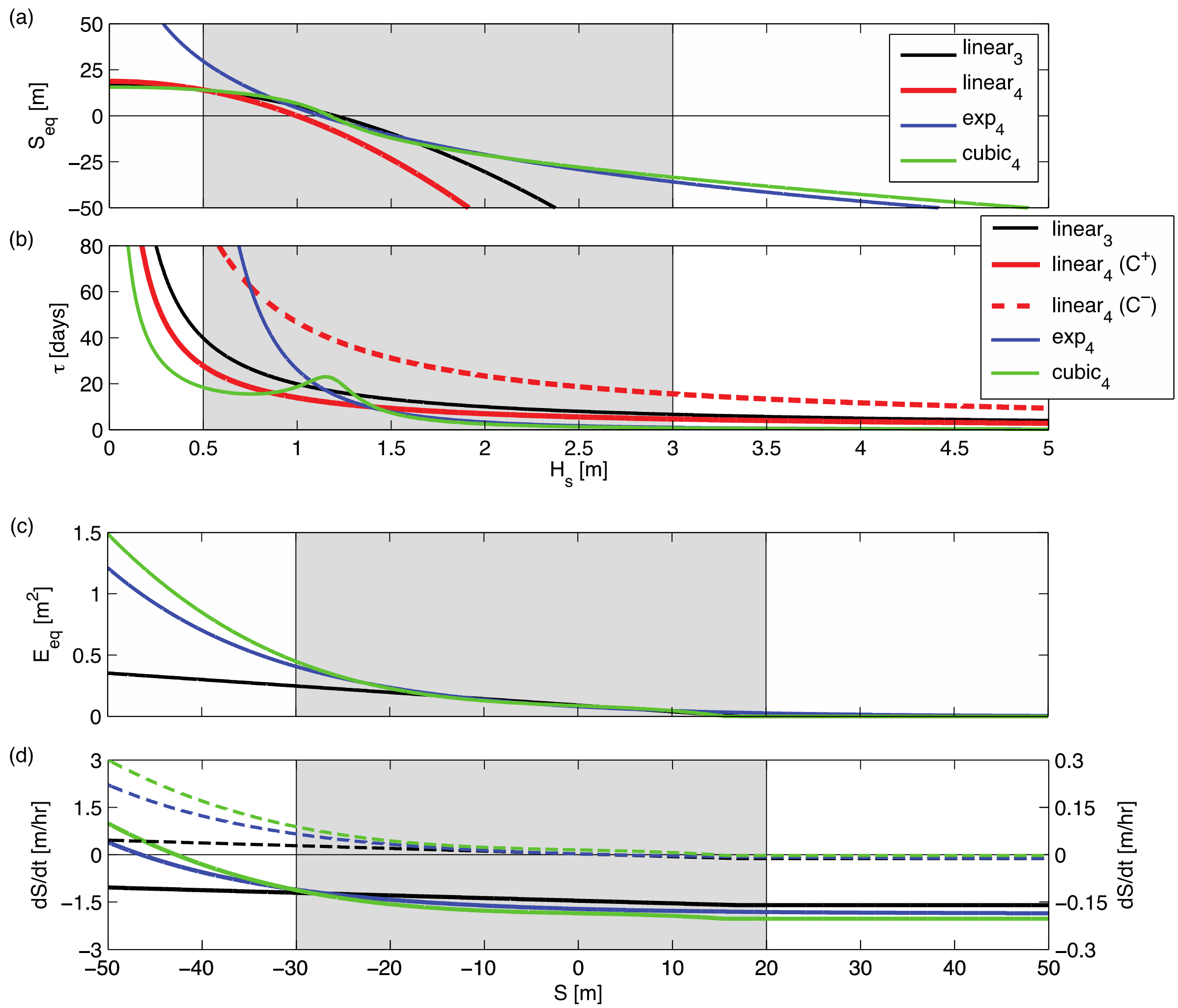


**Figure 10.** Example model results for Torrey Pines section T8 parameters: (a) equilibrium shoreline position $S_{eq}$, and (b) characteristic response time scale $\tau$, both versus significant wave height $H_s$. See legend for model types. (c) Model $E_{eq}$ and (d) shoreline change rate $dS/dt$, both versus shoreline position $S$. An accreted beach has $S > 0$ and an accreting beach has $dS/dt > 0$. In (d), results are shown for high ($H_s$ = 4 m; solid curves; left vertical axis) and low ($H_s$ = 0.4 m; dashed curves; right vertical axis) energy waves. Shading indicates the range of commonly occurring $H_s$ and $S$.